

Letter

# Neural Network Based Contact Force Control Algorithm for Walking Robots

Byeongjin Kim and Soohyun Kim \*

Department of Mechanical Engineering, KAIST, Daejeon 34141, Korea; geniuskpj@kaist.ac.kr

\* Correspondence: soohyun@kaist.ac.kr

**Abstract:** Walking algorithms using push-off improve moving efficiency and disturbance rejection performance. However, the algorithm based on classical contact force control requires an exact model or a Force/Torque sensor. This paper proposes a novel contact force control algorithm based on neural networks. The proposed model is adapted to a linear quadratic regulator for position control and balance. The results demonstrate that this neural network-based model can accurately generate force and effectively reduce errors without requiring a sensor. The effectiveness of the algorithm is assessed with the realistic test model. Compared to the Jacobian-based calculation, our algorithm significantly improves the accuracy of the force control. One step simulation was used to analyze the robustness of the algorithm. In summary, this walking control algorithm generates a push-off force with precision and enables it to reject disturbance rapidly.

**Keywords:** neural network; push-off; walking; force control; contact force; ground reaction force



**Citation:** Kim, B.; Kim, S. Neural Network Based Contact Force Control Algorithm for Walking Robot. *Sensors* **2021**, *21*, 287. <https://doi.org/10.3390/s21010287>

Received: 8 December 2020

Accepted: 28 December 2020

Published: 4 January 2021

**Publisher's Note:** MDPI stays neutral with regard to jurisdictional claims in published maps and institutional affiliations.



**Copyright:** © 2021 by the authors. Licensee MDPI, Basel, Switzerland. This article is an open access article distributed under the terms and conditions of the Creative Commons Attribution (CC BY) license (<https://creativecommons.org/licenses/by/4.0/>).

## 1. Introduction

Zero Moment Point (ZMP) control is widely accepted as a basic approach for walking robots [1–10]. Kajita [11] suggested a preview control system based on the Cart–Table model to generate biped walking patterns by ZMP. The preview control model requires the Center of Mass (CoM)'s height and weight to predict a stable CoM trajectory with the desired ZMP. However, the preview controller is not the most ideal for feedback because ZMP contains acceleration terms and also real-time feedback control in the influence of external disturbances is challenging. As described in Figure 1a, a ZMP-controlled robot swings its leg in order to take off and touches the leg down softly to the pre-defined footstep placement. When accelerating, a ZMP-controlled robot only uses its stance leg to accelerate, whereas humans utilize the propulsive push-off power from the swinging leg to accelerate [12,13] as shown in Figure 1b. The reason why the push-off mechanism is not used for ZMP-controlled robots is because push-off makes ZMP perturbation. Ground Reaction Forces (GRFs) from push-off are considered a disturbance, which is one of potential reasons for the efficiency gap between humans and robots [14–17]. Therefore, here we propose a new control method by push-off that does not cause ZMP perturbation [18].

Atrias [19,20] is a bipedal walking robot co-developed by Carnegie Mellon University and Oregon State University. The developers of Atrias have shown that Series Elastic Actuator (SEA) and Spring Loaded Inverted Pendulum (SLIP) model could improve the efficiency of walking. Atrias achieved a 9 km/h speed and robust walking on an uneven terrain with human like GRF. However, because GRF is controlled directly by the SLIP model, Atrias cannot stand still without making constant motion. Therefore, this solution is not applicable for robots that need to operate at a standstill. The researchers of Atrias calculated a required joint torque using the Jacobian method without using mass terms of foot.

A more complicated model does not guarantee a better performance because the uncertainties are coming from the model. Lee [21] used a null space method to regulate the GRF and kept the robot's balance. The null space method could control effectively

without a Force/Torque (F/T) sensor. Moreover, the performance is modulated by inertia information. Park [22] proposed a hybrid approach for contact force control combining the null space method and observer. The approach removes the effect of disturbance or error with the F/T sensor [23] by applying a filter or observer to reduce noise from sensed signal. Furthermore, the observer can estimate the force for sensorless control [24]. However, these approaches have delays that significantly reduce the performance and stability of the robots. the F/T sensor for bipedal robots is also high cost and weighs over 500 g.

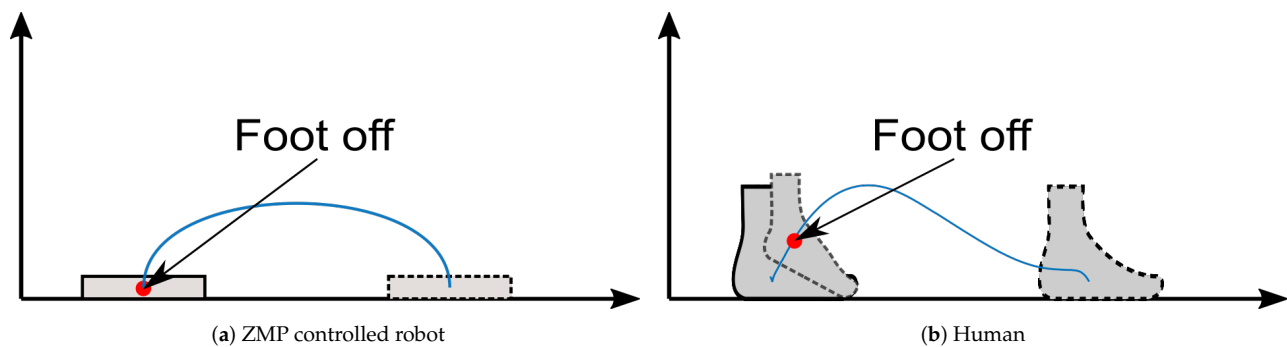


**Figure 1.** Swing leg's foot trajectory of (a) robot and (b) human during gait cycle. Robot's trajectory is from pre-developed robot [25]. Human gait is running at 3.56 m/s [26,27].

Neural network (NN) learning is a useful method for unknown complicated models [28,29]. NN-based hybrid position/force control was proposed by Passold [30] and Kumar [31]. Moreover, observer based approaches have been reported in [32–34]. However, these researches also used a force sensor in their model. Unlike sensor based control, Xu [35] suggested an impedance control based on an observer without force sensor. Adaption algorithm is applied to estimate stiffness and position of environment. Yet, this model has a significant delay for early contact.

In this paper, we propose a NN model to control ground reaction force without F/T sensor. This approach reduces modeling error and effort for finding model parameters. The contributions of our work are shown as follows:

- We propose a model based on neural network (NN) estimation on push-off force (GRF) control. It effectively decreases errors created by the robot's mass and gravity.
- The neural network model is applied with Linear Quadratic Regulator (LQR), which is adopted for balancing and generating desired force for push-off.
- We introduce the simulation to prove that our approach is validated in dynamic situations like walking.

The rest of the paper is organized as follows. Section 2 introduces the NN model and procedure of the simulation. Section 3 shows The results obtained from our model and simulation. The analysis about the result is summarized in Section 4. Section 5 concludes the paper.

## 2. Method

### 2.1. Neural Network Model

The parallel type leg in this paper is shown in Figure 2. It is developed for reducing inertia and fast walking. Physical modeling and simulation are executed on the MATLAB Simscape. There are two motors on the hip to control the position ( $x, z$ ) of the foot. The hip is connected to the body with a roll motor and is fixed during the NN training.

Dynamic equation for leg can be formulated as:

$$I\ddot{\theta} + C(\theta, \dot{\theta}) + K\theta + G(\theta) + J^T F = \tau \quad (1)$$

where  $I$  is the inertia matrix,  $C$  represents the coriolis and centrifugal term,  $K$  is the stiffness matrix and  $G(\theta)$  is the gravity function. The matrix  $J$  is the contact Jacobian for the contact position and  $F$  is the contact force matrix.  $\theta$  is the joint angle matrix and  $\tau$  is the joint torque matrix. If we know exact model, the reference torque for the desired force is obtained by:

$$\tau_{reference} = I\ddot{\theta}_m + C(\theta_m, \dot{\theta}_m) + K\theta_m + G(\theta_m) + J^T F_{desired} \quad (2)$$

where  $\theta_m$  represents the measured joint angle. Because the model information from CAD is not perfect, we need to conduct experiments for calculating the exact parameter [18]. Besides, links must be decomposed, and the test takes much time and effort. Furthermore, if we use a force sensor or observer to compensate the modeling error, the delay is unavoidable.

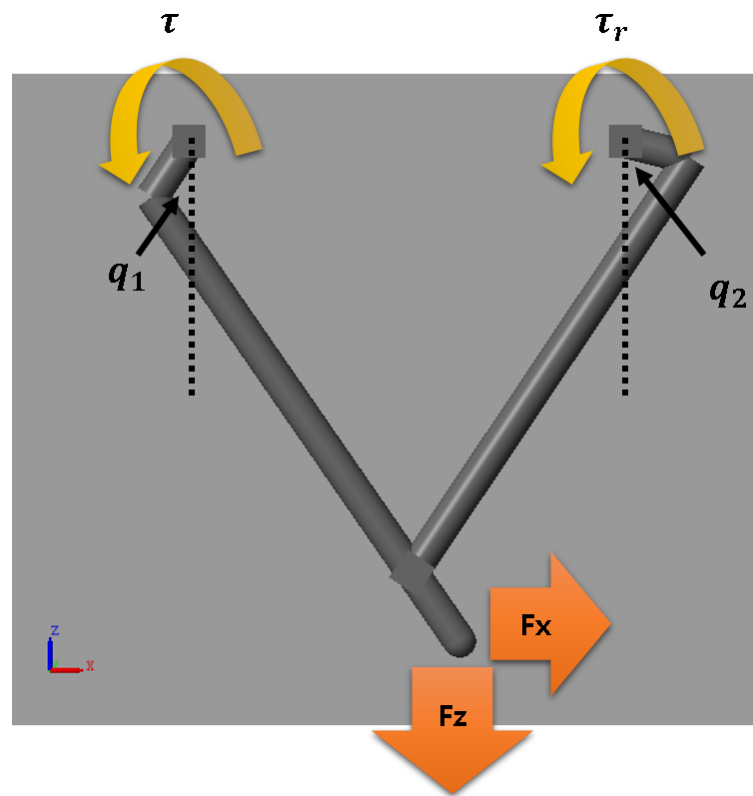


**Figure 2.** Leg model for neural network regression.

Thus, we propose a neural network model for removing model error without force sensor. Because the inertia of the leg is negligible against the body in this model,  $I$ ,  $C$  could be omitted. Then, the reference torque is simplified by:

$$\tau_{reference} = K\theta_m + G(\theta_m) + J^T F_{desired} = h(q_1, q_2, F_{dx}, F_{dz}) \quad (3)$$

where  $q_1, q_2$  are the joint angle from the left and right motors,  $F_{dx}, F_{dz}$  represents the x-axis and z-axis of the desired contact force. We assume the robot's foot is fixed on a vertically moving stage with a force sensor. When the torque ( $\tau, \tau_r$ ) is applied on the foot position by the joint angle ( $q_1, q_2$ ), we could measure the generated force  $F_x, F_z$ .

Our purpose is to acquire an approximation function of  $h$  by using these data. The neural network is efficient for curve fitting and works well in nonlinear regression. To avoid overfitting, the Bayesian regularization algorithm is adopted.

In Figure 3 and 4, the torque surface is plotted to determine the neural network parameter. The figures show  $h$  is not a highly nonlinear function. Therefore, we used one hidden layer. When the data are divided into 10 values in the range, sufficient performance is achieved. 10,000 datasets are collected under each  $10q_1 \times 10q_2 \times 10F_x \times 10F_z$ . Performance by random datasets is not significantly different. Ranges of input data are determined as follows:

$$F \in [-100, 100]N, q_1 \in [-\frac{\pi}{2}, 0]rad, q_2 \in [0, \frac{\pi}{2}]rad$$

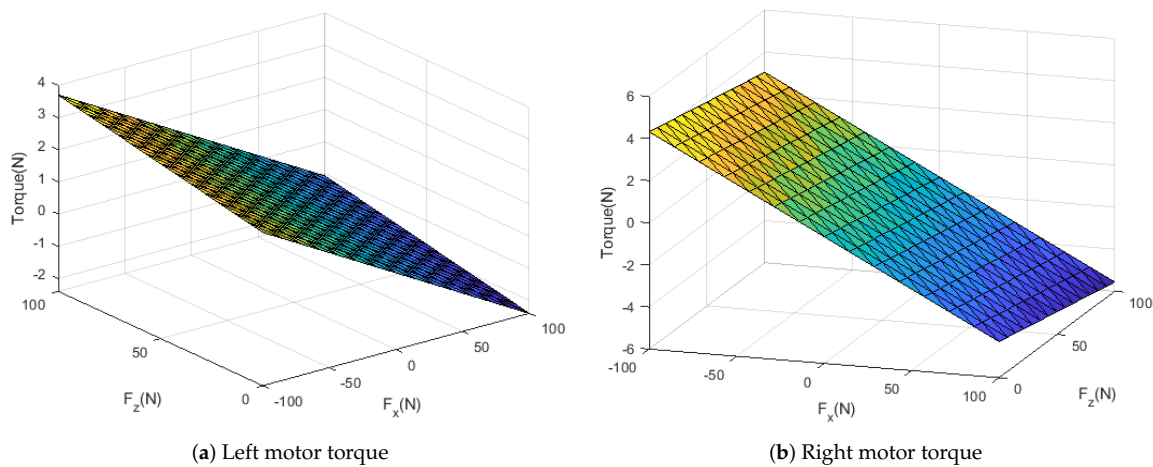


**Figure 3.** Measured torque is plotted for each force,  $q_1 = -\frac{\pi}{14}, q_2 = \frac{\pi}{14}$ .

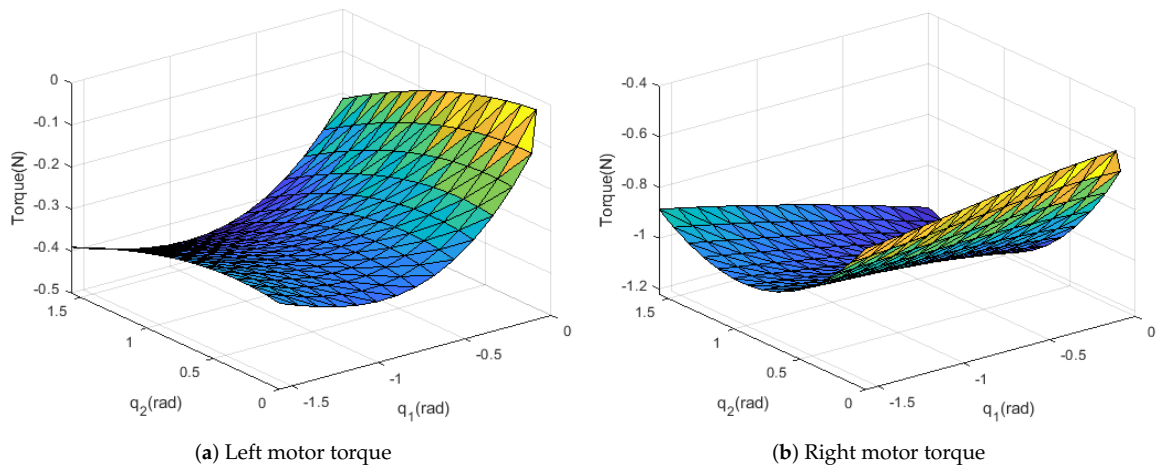


**Figure 4.** Measured torque is plotted for each joint angle,  $F_x = \frac{100}{7}N, F_z = \frac{100}{7}N$ .

The structure of the NN model is described in Figure 5 and in Equation (4).

$$y = b_2 + w_L * \text{tansig}(b_1 + w_I x) \quad (4)$$

- $y$  = output vector =  $[\tau \quad \tau_r]^T$ .
- $b_1, b_2$  = bias vector.
- $w_L$  = Layer weight matrix,  $w_I$  = Input weight matrix.
- $\text{tansig}(n) = \frac{2}{1+e^{-2n}} - 1$ .

- $x = \text{input vector} = [q_1 \quad q_2 \quad F_{dx} \quad F_{dz}]^T$ .

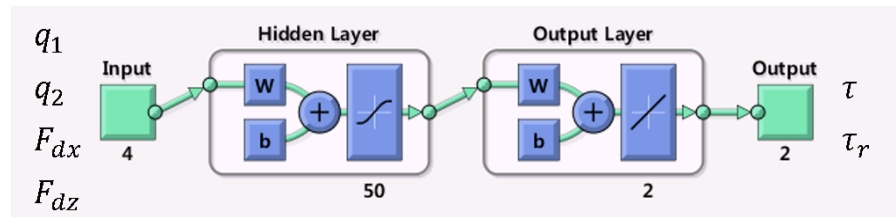


Figure 5. Neural network model for regression.

We used 70% of the data for training, 5% for validation, and 25% for the test. The parameters for NN learning are shown in Table 1. Training stops when the maximum number of epochs is reached,  $\mu$  exceeds  $\mu_{max}$  or the gradient falls below  $\text{min\_grad}$ .

Table 1. Parameters used for neural network training.

Parameters	Value	Description
epochs	1000	Maximum number of epochs
$\mu$	0.005	Marquardt adjustment parameter
$\mu_{dec}$	0.1	Decrease factor for $\mu$
$\mu_{inc}$	10	Increase factor for $\mu$
$\mu_{max}$	$1 \times 10^{10}$	Maximum value for $\mu$
$\text{min\_grad}$	$1 \times 10^{-7}$	Minimum performance gradient

## Cad Model

The same approach is tested on a realistic CAD model. It contains a motor, gearbox and it is fully designed for manufacturing. We assume this leg has the same workspace as a pre-developed robot [25]. The leg length is twice as long. The motor is selected for an increased length and weight. One motor position is changed because the motor is too big to place side by side. The range of  $q_1$  is not symmetric because the length of the left and right link are not the same.

$$F_x \in [-200, 200]N, F_z \in [-100, 1000]N, q_1 \in [0.82q_2 - 0.6067, 0.82q_2 + 0.52]rad, q_2 \in [0, 1.8]rad$$

## 2.2. Lqr Design

Figure 6 shows the 2D robot model and the parallel leg is simplified into a single effective link. LQR is an optimal feedback controller for a linear plant, and is easily tuned for multiple objectives by state (Q) and input (R) weight matrix.

The equations obtained from the model are shown below:

$$\begin{cases} M\ddot{x} = F_x \cos(q_b) \\ M\ddot{z} = F_z \cos(q_b) - Mg \end{cases} \quad \text{for body} \quad (5)$$

$$\begin{cases} R_x = -F_x \cos(q_b) \\ R_z = Mg - F_z \cos(q_b) \\ q_b = q_l - q_h \\ I\ddot{q}_l = R_x l \cos(q_l) - R_z l \sin(q_l) \end{cases} \quad \text{for leg}$$

- $M$  = mass of robot,  $g$  = gravity acceleration.
- $F$  = force from leg to body.
- $R$  = force from body to leg.
- $q_b$  = body angle,  $q_h$  = hip angle,  $q_l$  = leg angle.
- $I$  = inertia of robot,  $l$  = length from body to foot.

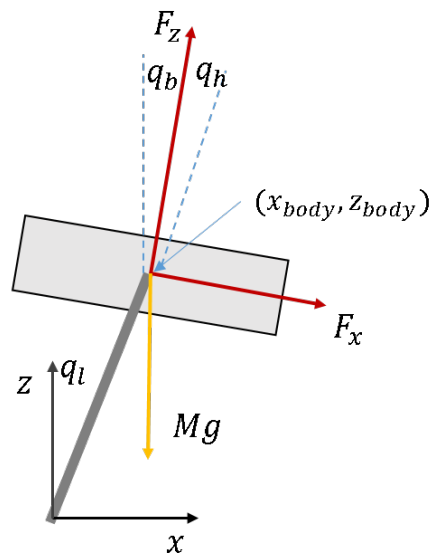


Figure 6. Free body diagram for body.

Besides high gain being applied in the support phase, we assume  $l$  is constant. The mass of the leg is  $\frac{1}{20}$  scale of robot mass, thus it is ignored. At a linearized point,  $q_b^* = q_l^* \approx 0$ . The state-space equation for LQR can be written as:

$$\begin{aligned}
 H\dot{X} &= AX + BU \\
 \dot{X} &= H^{-1}(AX + BU) = A'X + B'U \\
 X &= [q_b \quad \dot{q}_b \quad x \quad \dot{x} \quad z \quad \dot{z}]^T \\
 H &= \text{diag}([1 \quad I \quad 1 \quad M \quad 1 \quad M]) \\
 A &= \begin{bmatrix} 0 & 1 & 0 & 0 & 0 & 0 \\ 0 & 0 & 0 & 0 & 0 & 0 \\ 0 & 0 & 0 & 1 & 0 & 0 \\ 0 & 0 & 0 & 0 & 0 & 0 \\ 0 & 0 & 0 & 0 & 0 & 1 \\ 0 & 0 & 0 & 0 & 0 & 0 \end{bmatrix} \\
 B &= \begin{bmatrix} 0 & 0 \\ -l & 0 \\ 0 & 0 \\ 1 & 0 \\ 0 & 0 \\ 0 & 1 \end{bmatrix} \\
 U &= [F_x \quad F_z]^T
 \end{aligned} \tag{6}$$

We use simple PD control on hip roll motors.

$$u_{roll} = K_P(q_{ref} - q_{roll}) - K_D\dot{q}_{roll} \tag{7}$$

$q_{roll}$  = angle of roll motor,  $\dot{q}_{roll}$  = angular velocity of roll motor,  $q_{ref}$  = reference angle  $q_{ref}$  is a constant that keeps initial hip roll angle.

$$\begin{aligned}
 K_{lqr} &= \begin{bmatrix} 100 & 10 & 50,000 & 5000 & 0 & 0 \\ 0 & 0 & 0 & 0 & 50,000 & 5000 \end{bmatrix} \\
 U &= -K_{lqr}X
 \end{aligned} \tag{8}$$

$K_{lqr}$  is calculated from  $(A, B, Q, R)$  by the algebraic Riccati equation. The controllability matrix is not full rank but is stabilizable. It means that the robot could fall from some initial states. Controlling  $x$  and  $q_b$  are trade-offs because two states are coupled. If we give too much weight to  $x$ ,  $q_b$  is not controlled properly. After some simulation, we could find appropriate ratio for them.

The entire control flow is described as:

1. LQR calculates desired contact force  $(F_x, F_z)$  from error.
2. Desired Joint torque  $(\tau, \tau_r)$  is obtained from a neural network regression model.
3. Apply the joint torque to the robot plant and measure the states.

Workflow is also described in Figure 7.

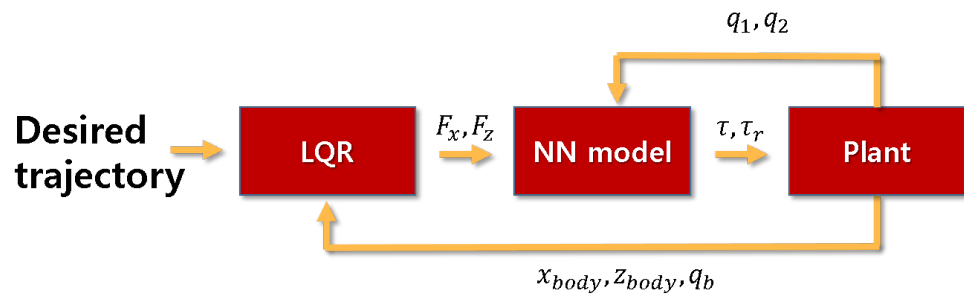


Figure 7. Entire control flow, NN means neural network model.

### 2.3. One Step Simulation

We establish a simulation model to verify that the proposed approach works well while the robot body is moving. The robot model is demonstrated in Figure 8. There are two hip roll motors on the invisible frame. The control objective for the hip roll motor is to sustain the angle. There is no external constraint on the model, but only spatial contacts between the spherical foot and ground. The static friction coefficient is 1 and the dynamic is 0.8. This is the friction coefficient of rubber on dry concrete. The hip width is 0.1m and the other parameters are written in Figure 9 and Table 2.

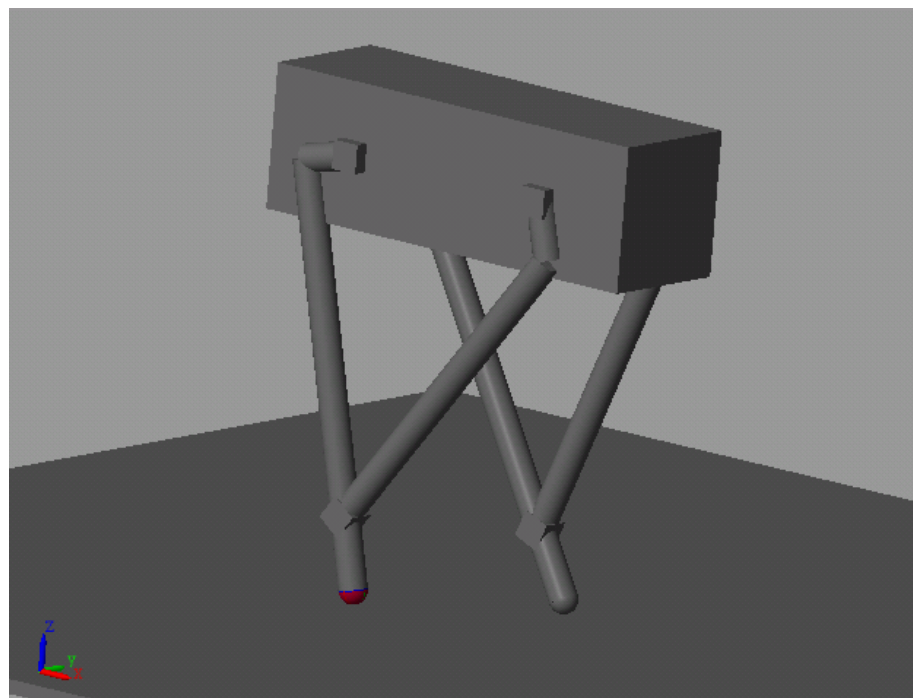


Figure 8. Robot model for Simscape.

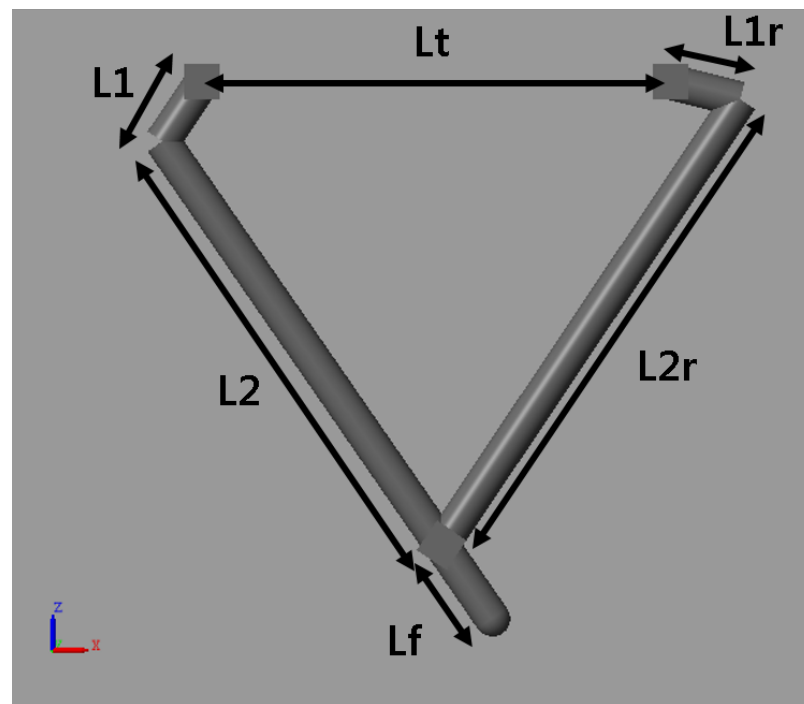


Figure 9. Leg model parameter.

Table 2. Leg model parameter table.

Name	Value
$L1$ (m)	0.04
$L1r$ (m)	0.04
$L2$ (m)	0.24
$L2r$ (m)	0.255
$Lf$ (m)	0.05
$Lt$ (m)	0.08
$M$ (kg)	10

Leg length parameters are optimized for minimizing the required torque, and the step width is 0.1 m. The push-off force is generated by trajectory based on the trigonometric function ( $p_{desired} = \frac{A}{2}(1 - \cos(\frac{2\pi t}{T}))$ ). The maximum force for the z-axis is 170% of the mass and force for the x-axis is 40%. The step time and amplitude of the push-off is selected by tuning.

Simulation starts from the double support phase. Right leg push-off ground and mode is changed into a single support phase. Body angle and effective leg length  $l$  are regulated in a single support phase. After heel-strike, the robot is balanced.

### 3. Results

#### 3.1. Neural Network Model

We did the test to prove robustness:

1. Pick random desired force.
2. Calculate the joint torque by using a neural network model.
3. Compare the real torque for the desired force with a calculated one (Test 1).
4. Apply the joint torque and compare the measured force with the desired (Test 2).

Figure 10 shows the logarithmic MSE decrease as the number of neurons increases. However, neurons more than 50 show negligible performance improvement in force generation (Test 2). Thus, we decide the number of neurons is 50 and it needs about 27 ms to calculate torque.



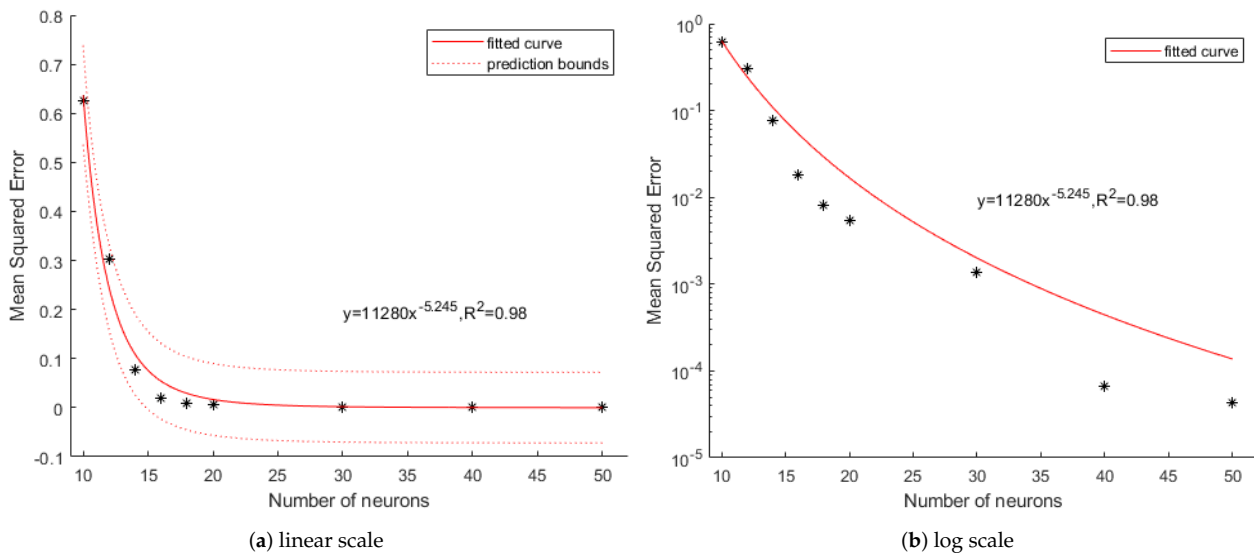


Figure 10. Mean square error of torque by the number of neurons.

Test 1 executed 1000 times and Test 2 executed 100 times. When we use the Jacobian method, torque is calculated by  $\tau_{reference} = J^T F_{desired}$ . The gravitational term is not applied because we assume the mass model is not accurate. In the error histogram (Figure 11a), the torque error from the NN model is much lower than the error from the Jacobian method. Table 3 shows the predicted torque error by dismissing  $I, C$ . In Test 2, the mean error from the Jacobian method is 4.58 N and the mean error from NN is 0.37 N. The mean error is reduced by 92% when a neural network model is applied.

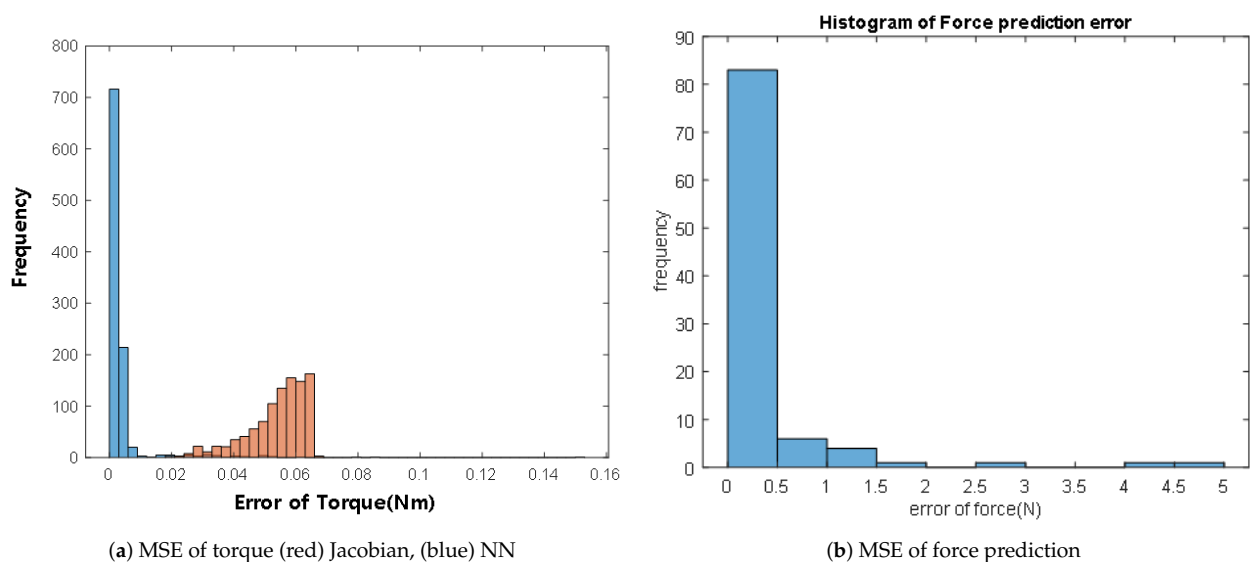


Figure 11. Histogram of mean square error.

Table 3. Statistical value of prove test.

	Test 1 (Nm)	Test 2 (N)
MSE	$9.45 \times 10^{-5}$	0.67
Mean	0.0039	0.37
STD	0.0089	0.74

### CAD Model

To prove the robustness of the NN model, Test 2 is applied to the CAD model. The root mean squared error (RMSE) from the NN model is 73.7% lower than the Jacobian method. Because the CAD model is heavier (4.5 kg) than simplified model (300 g), Figure 12 shows increased force error. The moving average line indicates the error from NN is significantly smaller than the Jacobian's.

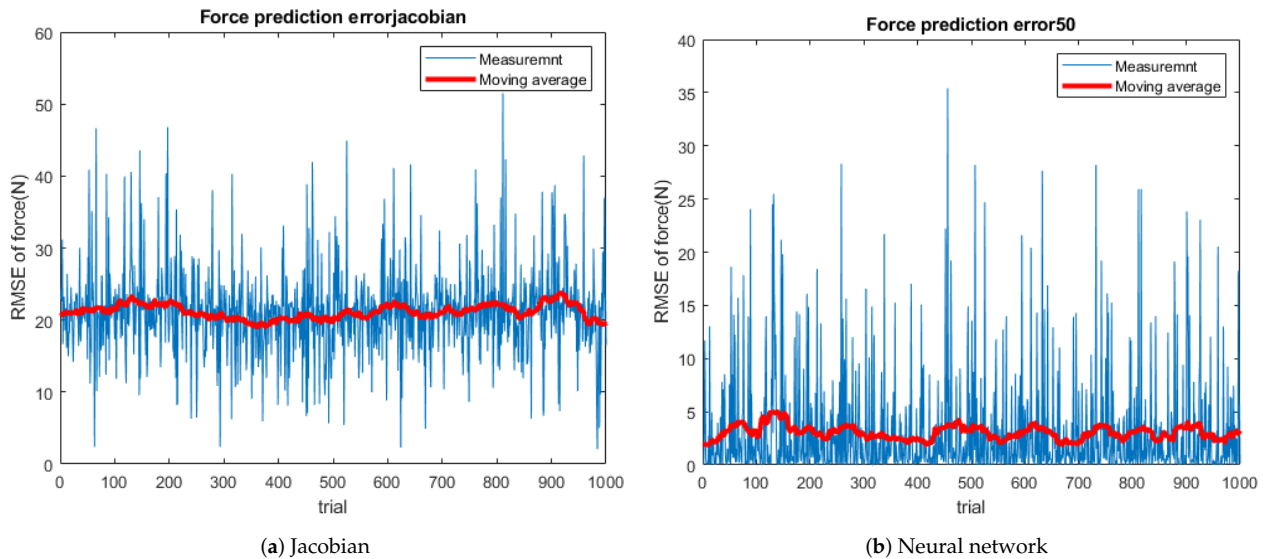


Figure 12. Force prediction error.

According to Figure 13 and Table 4, the average error is reduced by 85.6%. There are some spikes over 10 N in the NN model. When the leg is almost fully stretched, the spikes appear by a singularity. Simscape solver's linearization and approximation also make an error.

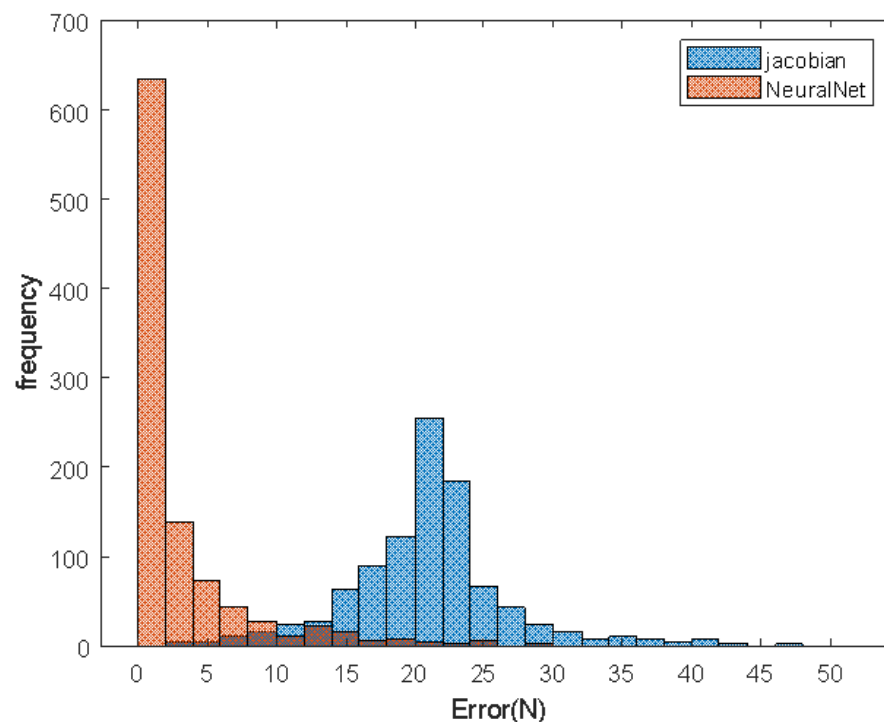


Figure 13. Histogram of force prediction error.

**Table 4.** Statistical value of prove test in CAD model.

Error	Max (N)	Avg (N)	Var (N)	RMSE (N)
Jacobian	51	21.2	36.2	22.0
Neural	36	3.1	24.2	5.8
Change (%)	−29.4	−85.6	−33.1	−73.7

### 3.2. One Step Simulation

Figure 14 demonstrates the procedure of one step simulation. Figure 15 indicates the states and input of the LQR controller. Heel strike occurs at 0.6 s and the robot keeps balance without additional stepping. On the other hand, Atrias has no ability to keep balance at standstill [20]. It is critical for robots with manipulator.

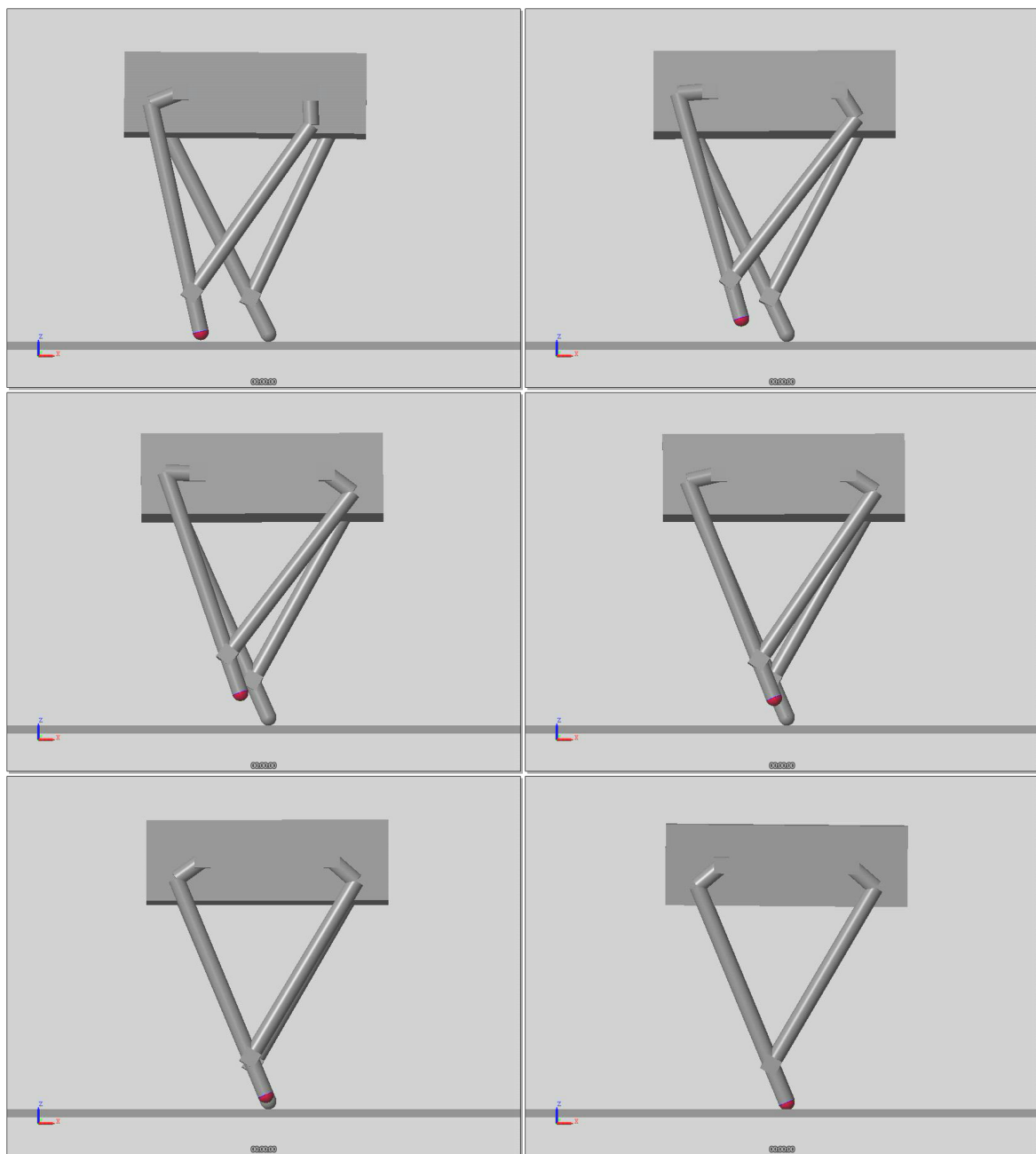
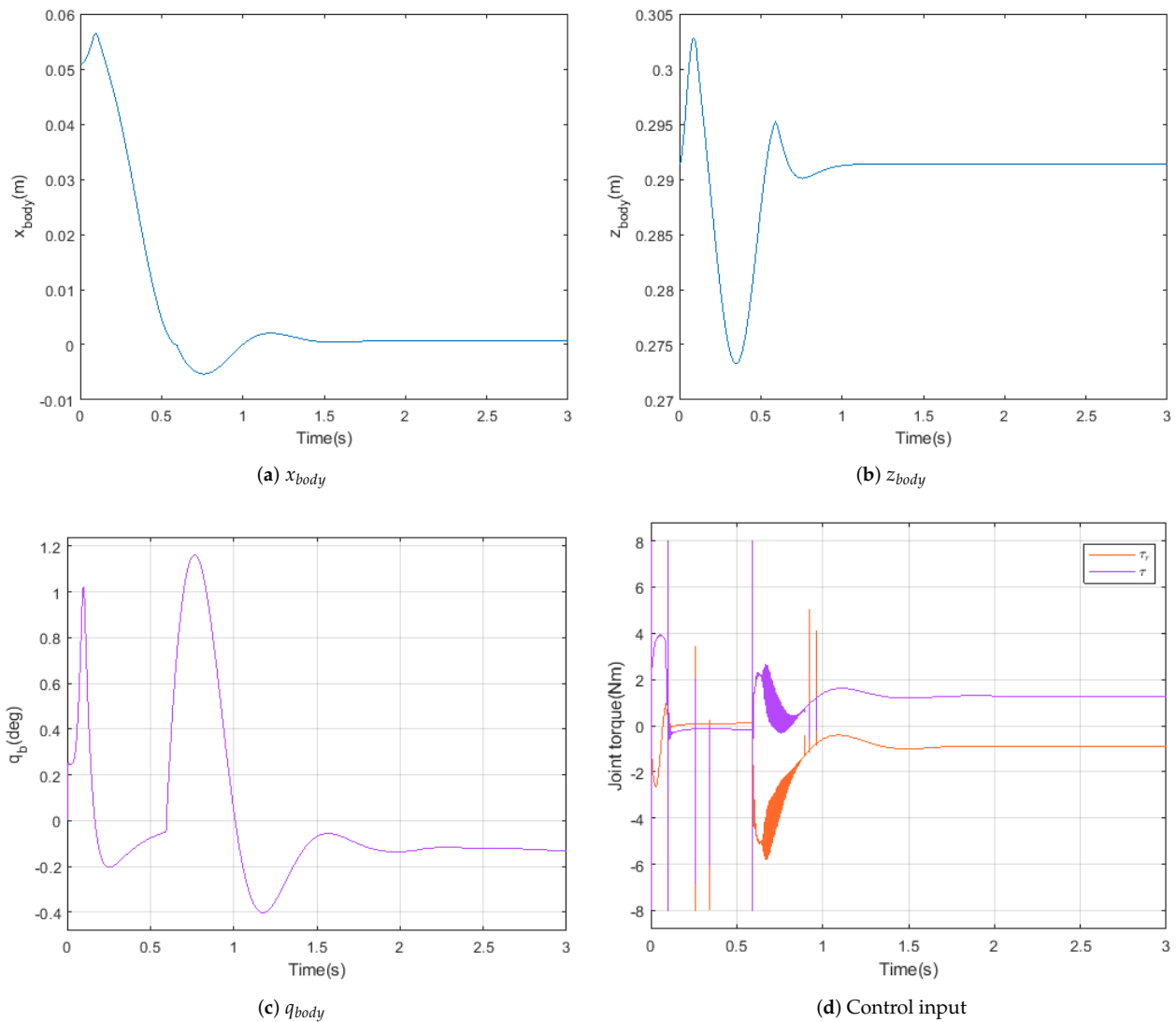
**Figure 14.** Still shot of one step simulation.

Figure 15a,b show the movement of the body, taking maximum overshoot values of 1 cm and 2 cm. Figure 15c shows the response of the body angle  $q_b$ , which takes values between  $-0.4$  and  $1.2$  degrees. The joint torque of the swing foot, having maximum values of  $-8$  and  $8$  Nm, are presented in Figure 15d. Peak values appeared by mode transition and numerical error of simulation.



**Figure 15.** States and input of swing foot.

Figure 16 shows the real and target normal force of the stance leg. The NN model operates normally under moving conditions. Average error is 0.64 N.

In Figure 17a, GRF is not measured in the swing phase. Human's GRF is drawn for a stance leg from heel strike to push-off [36]. It needs more steps to draw the grf of the stance leg. Hence, we draw similar results by adding the swing and stance leg's normal force.

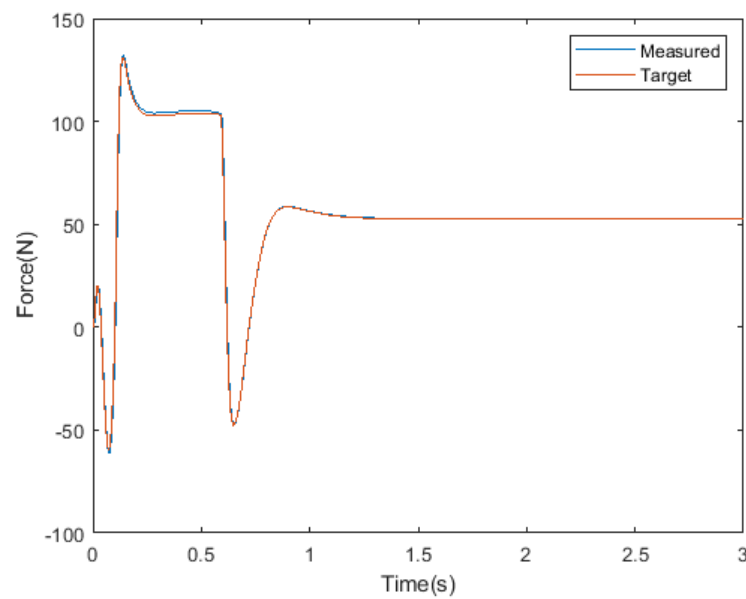


Figure 16. Measured and desired force.

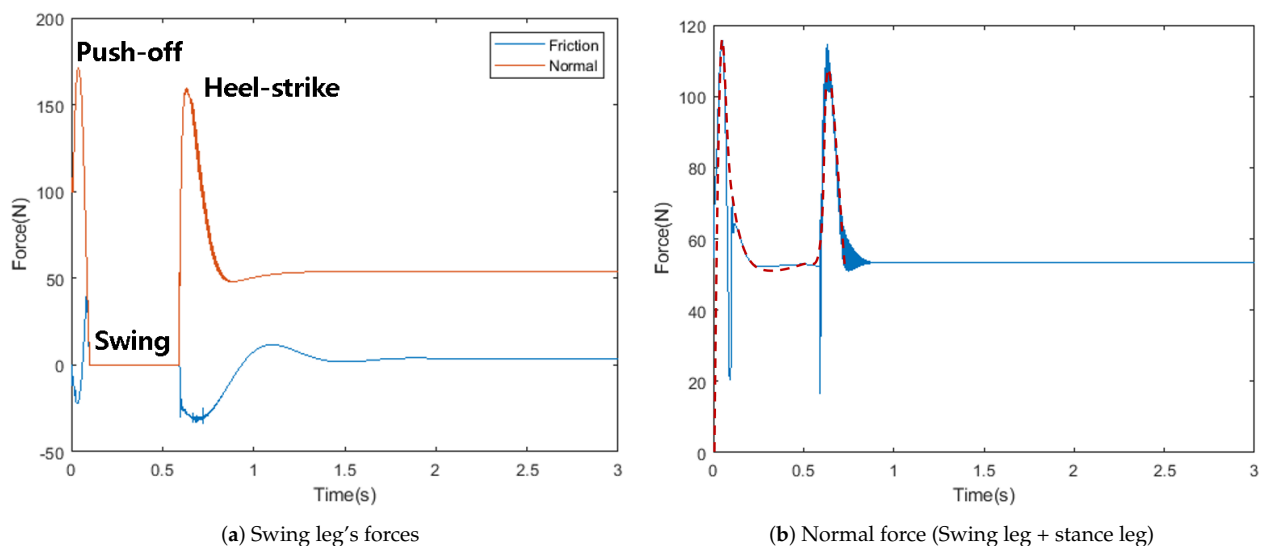


Figure 17. Normal and friction force of one step simulation. Red dashed line: approximation of sum.

#### 4. Discussion

The neural network model has a high accuracy in force control. The average and RMS error are smaller than 10 N. According to Table 4, the proposed model achieves better accuracy than the Jacobian method without including mass information. The NN model removes the time-consuming process of formulating equations and finding the parameters of each link. In biped robots, the error is produced by bolts, bearings, wire and electronic parts. Even though all terms are modeled, force control error always exists [21]. NN modeling is a systematic approach to modify models by experiments and learning. The main reason for performance improvement comes from dismissing gravitational terms in the Jacobian method. Since we designed the leg for faster movement, the leg mass under 5 Kg was used. There will be more improvement for heavier legs. In the manipulator's case, a computed torque method or observer based approach is applied for better performance and removing the model error. Due to the noisy value from sensors, a filter or observer is used in those approaches. Stability and performance deteriorate because the delay is

accompanied by filters. Unlike manipulators, walking robots could fall by a small delay. F/T sensors for an observer are also expensive and heavy.

Since Equation (3) has no terms about ground, the NN model is not affected by the condition and material of the ground. Therefore, the model is also working in a floating state. Figure 3 shows the model is linear about  $F_z$ . Thus,  $F_z$  range for the dataset could be from 0 to positive value. If we get data only for pushing ground, it does not have any performance drop.

Based on the results in Section 3.2, our approach can be used for moving platforms. Figure 17b shows an approximated line that resembles a human's GRF. There is a flat part between two peaks in the single support phase. Because the robot's speed is 0.25 m/s which is much slower than a human's (1–1.5 m/s), using push-off, the robot could achieve more speed for multiple step. Although push-off and heel strike are disturbances over 100 N, the proposed LQR controller rejects the disturbance with a small error. Robots could stand without any motion or additional stepping. ZMP-controlled robots usually need an F/T sensor or advanced control like a capture point to remove disturbance.

## 5. Conclusions

The purpose of this article is to provide a new contact force control algorithm. Unknown disturbance and modeling error will cause the failure of the walking robot. We propose a NN based force control method to solve these problems. We use NN regression to remove time-consuming steps like formulating equations and finding parameters for model. Secondly, we introduce the LQR walking controller with the NN model for balancing and push-off.

The performance of contact force generation was compared with the Jacobian method. The result shows that the neural network model significantly improves the performance of force control. The research pointed out that the proposed method is highly applicable for contact force control. Our approach has strong robustness on one step simulation which contains transient disturbance. The proposed algorithm satisfies requirements under simulation and the result shows the feasibility of applying our approach to walking control.

NN modeling can be easily implemented by other manipulators or robots. The advantage of these solutions can be exploited well on complicated multi-axis robots or parallel manipulators.

In our future work, we will add frictional or damping terms in the model. Friction modeling is a challenging problem to be added to force control. However, this is essential to improve performance in walking of real robots. The redundant degree of freedom will be considered later. Additional objects like torque minimization can be added to the model.

**Author Contributions:** Conceptualization, B.K. and S.K.; methodology, B.K.; software, B.K.; writing—original draft preparation, B.K.; writing—review and editing, B.K. All authors have read and agreed to the published version of the manuscript.

**Funding:** This research was funded by Korea Hydro & Nuclear Power Co., Ltd. Project name is 'Development of Visual Inspection Robot for Essential Service Water Piping' grant number N06200049.

**Institutional Review Board Statement:** Not applicable.

**Informed Consent Statement:** Not applicable.

**Data Availability Statement:** Data available on request due to restrictions by funding organization.

**Conflicts of Interest:** The authors declare no conflict of interest.

## Abbreviations

The following abbreviations are used in this manuscript:

NN	Neural Network
GRF	Ground Reaction Force
CoM	Center of Mass
LQR	Linear Quadratic Regulator
F/T	Force Torque
CAD	Computer Aided Design
ZMP	Zero Moment Point

## References

- Morisawa, M.; Kajita, S.; Kanehiro, F.; Kaneko, K.; Miura, K.; Yokoi, K. Balance control based on Capture Point error compensation for biped walking on uneven terrain. In Proceedings of the 2012 12th IEEE-RAS International Conference on Humanoid Robots (Humanoids 2012), Osaka, Japan, 29 November–1 December 2012; pp. 734–740. [\[CrossRef\]](#)
- Englsberger, J.; Ott, C. Integration of vertical COM motion and angular momentum in an extended Capture Point tracking controller for bipedal walking. In Proceedings of the 2012 12th IEEE-RAS International Conference on Humanoid Robots (Humanoids 2012), Osaka, Japan, 29 November–1 December 2012; pp. 183–189. [\[CrossRef\]](#)
- Shafiee-Ashtiani, M.; Yousefi-Koma, A.; Shariat-Panahi, M.; Khadiv, M. Push recovery of a humanoid robot based on model predictive control and capture point. In Proceedings of the 2016 4th International Conference on Robotics and Mechatronics (ICROM), Tehran, Iran, 26–28 October 2016; pp. 433–438. [\[CrossRef\]](#)
- Sugihara, T.; Yamamoto, T. Foot-guided agile control of a biped robot through ZMP manipulation. In Proceedings of the 2017 IEEE/RSJ International Conference on Intelligent Robots and Systems (IROS), Vancouver, BC, Canada, 24–28 September 2017; pp. 4546–4551. [\[CrossRef\]](#)
- Ishiguro, Y.; Kojima, K.; Sugai, F.; Nozawa, S.; Kakiuchi, Y.; Okada, K.; Inaba, M. Bipedal oriented whole body master-slave system for dynamic secured locomotion with LIP safety constraints. In Proceedings of the 2017 IEEE/RSJ International Conference on Intelligent Robots and Systems (IROS), Vancouver, BC, Canada, 24–28 September 2017; pp. 376–382. [\[CrossRef\]](#)
- Kuindersma, S.; Permenter, F.; Tedrake, R. An efficiently solvable quadratic program for stabilizing dynamic locomotion. In Proceedings of the 2014 IEEE International Conference on Robotics and Automation (ICRA), Hong Kong, China, 31 May–7 June 2014; pp. 2589–2594. [\[CrossRef\]](#)
- Caron, S.; Pham, Q.; Nakamura, Y. ZMP Support Areas for Multicontact Mobility Under Frictional Constraints. *IEEE Trans. Robot.* **2017**, *33*, 67–80. [\[CrossRef\]](#)
- Kamioka, T.; Kaneko, H.; Takenaka, T.; Yoshiike, T. Simultaneous Optimization of ZMP and Footsteps Based on the Analytical Solution of Divergent Component of Motion. In Proceedings of the 2018 IEEE International Conference on Robotics and Automation (ICRA), Brisbane, Australia, 21–25 May 2018; pp. 1763–1770. [\[CrossRef\]](#)
- Kim, J.H.; Lee, J.; Oh, Y. A Theoretical Framework for Stability Regions for Standing Balance of Humanoids Based on Their LIPM Treatment. *IEEE Trans. Syst. Man Cybern. Syst.* **2020**, *50*, 4569–4586. [\[CrossRef\]](#)
- Yu, Z.; Zhou, Q.; Chen, X.; Li, Q.; Meng, L.; Zhang, W.; Huang, Q. Disturbance Rejection for Biped Walking Using Zero-Moment Point Variation Based on Body Acceleration. *IEEE Trans. Ind. Inform.* **2019**, *15*, 2265–2276. [\[CrossRef\]](#)
- Kajita, S.; Kanehiro, F.; Kaneko, K.; Fujiwara, K.; Harada, K.; Yokoi, K.; Hirukawa, H. Biped walking pattern generation by using preview control of zero-moment point. In Proceedings of the IEEE International Conference on Robotics and Automation, Taipei, Taiwan, 14–19 September 2003; Volume 2, pp. 1620–1626. [\[CrossRef\]](#)
- Zelik, K.E.; Takahashi, K.Z.; Sawicki, G.S. Six degree-of-freedom analysis of hip, knee, ankle and foot provides updated understanding of biomechanical work during human walking. *J. Exp. Biol.* **2015**, *218*, 876–886. [\[CrossRef\]](#) [\[PubMed\]](#)
- Soo, C.H.; Donelan, J.M. Mechanics and energetics of step-to-step transitions isolated from human walking. *J. Exp. Biol.* **2010**, *213*, 4265–4271. [\[CrossRef\]](#)
- Collins, S. Dynamic Walking Principles Applied to Human Gait. Ph.D. Thesis, The University of Michigan, Ann Arbor, MI, USA, 2008.
- Huang, T.W.; Shorter, K.; Adamczyk, P.; Kuo, A. Mechanical and energetic consequences of reduced ankle plantarflexion in human walking. *J. Exp. Biol.* **2015**, *218*. [\[CrossRef\]](#)
- Collins, S.; Kuo, A. Recycling Energy to Restore Impaired Ankle Function during Human Walking. *PLoS ONE* **2010**, *5*, e9307. [\[CrossRef\]](#)
- Zelik, K.E. Is the Foot Working With or Against the Ankle During Human Walking? In Proceedings of the Dynamic Walking Conference, Columbus, OH, USA, 21–24 July 2015.
- Park, H.W.; Sreenath, K.; Hurst, J.; Grizzle, J. Identification of a Bipedal Robot with a Compliant Drivetrain. *IEEE Control Syst.* **2011**, *31*, 63–88. [\[CrossRef\]](#)
- Spring-Mass Walking with ATRIAS in 3D: Robust Gait Control Spanning Zero to 4.3 KPH on a Heavily Underactuated Bipedal Robot. In Proceedings of the ASME 2015 Dynamic Systems and Control Conference, Columbus, OH, USA, 28–30 October 2015.

20. Hubicki, C.M.; Abate, A.; Clary, P.; Rezazadeh, S.; Jones, M.S.; Peekema, A.; Why, J.V.; Domres, R.; Wu, A.; Martin, W.; et al. Walking and Running with Passive Compliance: Lessons from Engineering: A Live Demonstration of the ATRIAS Biped. *IEEE Robot. Autom. Mag.* **2018**, *25*, 23–39. [[CrossRef](#)]
21. Lee, Y.; Hwang, S.; Park, J. Balancing of humanoid robot using contact force/moment control by task-oriented whole body control framework. *Auton. Robots* **2016**, *40*. [[CrossRef](#)]
22. Park, J.; Khatib, O. Robot multiple contact control. *Robotica* **2008**, *26*, 667–677. [[CrossRef](#)]
23. Bouyarmane, K.; Chappellet, K.; Vaillant, J.; Kheddar, A. Quadratic Programming for Multirobot and Task-Space Force Control. *IEEE Trans. Robot.* **2019**, *35*, 64–77. [[CrossRef](#)]
24. Nagai, S.; Kawamura, A. Position/Force Sensorless Force Control Using Reaction Force Observer for Compact Dual Solenoid Actuator. In Proceedings of the IECON 2019—45th Annual Conference of the IEEE Industrial Electronics Society, Lisbon, Portugal, 14–17 October 2019; Volume 1, pp. 3635–3640. [[CrossRef](#)]
25. Song, B. The Robot For Nuclear Plant. *Korea JoongAng Daily*, 26 April 2018. Available online: <https://news.joins.com/article/22569622> (accessed on 31 December 2020).
26. Dorn, T.; Lin, Y.C.; Pandy, M. Estimates of muscle function in human gait depend on how foot-ground contact is modelled. *Comput. Methods Biomech. Biomed. Eng.* **2011**, *15*, 657–668. [[CrossRef](#)] [[PubMed](#)]
27. Dorn, T.; Schache, A.; Pandy, M. Muscular strategy shift in human running: Dependence of running speed on hip and ankle muscle performance. *J. Exp. Biol.* **2012**, *215*, 1944–1956. [[CrossRef](#)]
28. Lewis, F.; Ge, S. *Neural Networks in Feedback Control Systems*; John Wiley & Sons, Inc.: Hoboken, NJ, USA, 2006; pp. 791–825. [[CrossRef](#)]
29. Puga-Guzmán, S.; Moreno-Valenzuela, J.; Santibañez, V. Adaptive Neural Network Motion Control of Manipulators with Experimental Evaluations. *Sci. World J.* **2014**, *2014*, 694706. [[CrossRef](#)] [[PubMed](#)]
30. Passold, F.; Stemmer, M. Force Control of a Scara Robot Using Neural Networks. In Proceedings of the Fourth International Workshop on Robot Motion and Control (IEEE Cat. No.04EX891), Puzszykowo, Poland, 20 June 2004; pp. 247–252. [[CrossRef](#)]
31. Kumar, N.; Panwar, V.; Nagarajan, S.; Sharma, S.; Borm, J.H. Neural network based hybrid force/position control for robot manipulators. *Int. J. Precis. Eng. Manuf.* **2011**, *12*, 419–426. [[CrossRef](#)]
32. Piao, J.; Kim, E.S.; Choi, C.S.; Moon, C.B.; Park, M.H. Indirect Force Control of a Cable-Driven Parallel Robot: Tension Estimation using Artificial Neural Network trained by Force Sensor Measurements. *Sensors* **2019**, *19*, 2520. [[CrossRef](#)]
33. Wahrburg, A.; Bös, J.; Listmann, K.D.; Dai, F.; Matthias, B.; Ding, H. Motor-Current-Based Estimation of Cartesian Contact Forces and Torques for Robotic Manipulators and Its Application to Force Control. *IEEE Trans. Autom. Sci. Eng.* **2018**, *15*, 879–886. [[CrossRef](#)]
34. Li, C.; Zhang, Z.; Xia, G.; Xie, X.; Zhu, Q. Efficient Force Control Learning System for Industrial Robots Based on Variable Impedance Control. *Sensors* **2018**, *18*, 2539. [[CrossRef](#)]
35. Xu, W.; Cai, C.; Zou, Y. Neural-network-based robot time-varying force control with uncertain manipulator–environment system. *Trans. Inst. Meas. Control* **2014**, *36*, 999–1009. [[CrossRef](#)]
36. Geyer, H.; Seyfarth, A.; Blickhan, R. Compliant leg behavior explains basic dynamics of walking and running. *Proc. Biol. Sci. R. Soc.* **2006**, *273*, 2861–2867. [[CrossRef](#)] [[PubMed](#)]